Available online at www.sciencedirect.com
ScienceDirect
Optics Communications 281 (2008) 3522–3526
OPTICS COMMUNICATIONS
www.elsevier.com/locate/optcom

Thermal stress effects of the diode-end-pumped Nd:YLF slab

Zhe Ma [a,*], Jiancun Gao [a], Daijun Li [b], Junlin Li [a], Nianle Wu [a], Keming Du [b]

[a] Department of Physics, Tsinghua University, Beijing 100084, China
[b] EdgeWave GmbH, Schumanstrasse 18B, Würselen 52146, Germany

Received 30 October 2007; received in revised form 7 March 2008; accepted 7 March 2008

Abstract

The thermal stress effects of the diode-end-pumped Nd:YLF slab laser crystals are numerically investigated. The theoretical model is established by considering the divergence of the pump beam in the slab and the additional heat generated in the upconversion. Using the three dimensional finite element analyses, accurate numerical solutions based on the theoretical model are achieved. Our analyses focuses on the thermal fracture damage of the Nd:YLF slab under both the lasing and non-lasing conditions, and the predicted values are compared with the experimental results.

Keywords: Nd:YLF; Diode-pumped lasers; Thermal stress

1. Introduction

Diode-pumped solid-state lasers are considered outstanding because of their high efficiency, compact package and beam quality [1]. However, output power scalability and beam quality in most of the solid-state lasers are limited by the thermal lensing and the thermal fracture damage of lasing gain medium. Nd:YLF has demonstrated that it is a very good laser crystal for generating high-energy *Q*-switched pulses because of its nature birefringence and its long storage time on upper laser level. With the increasing temperature, YLF shows a decrease of refractive index, and creates a negative thermal lens which partly compensates for the positive lens due to the bulging of the slab end face [2]. The relatively weak thermal lens gives Nd:YLF a significant advantage for power scaling of diode-pumped system into multiwatt region while retaining good beam quality. But the small tensile strength of Nd:YLF limits the maximum average pump power on the crystal. The consequence of larger thermal stresses, while the pump power increases, is caused by the increased heat load in the slab. Ultimately, with a sufficient heat load, slab fracture will occur.

Partially end-pumped slab lasers with a stable–unstable hybrid resonator have been proven to be a favorable concept for power scaling at high beam quality and efficiency because they have both the properties of the high overlapping efficiency of end-pumped rod lasers and the excellent cooling conductivity of slab lasers [3–9]. The Nd:YLF slabs end-pumped by the multi-bar diode stacks are widely used in this end-pumped slab configuration [7–9]. The Nd:YLF slab is pumped by pulsed or CW diode stack and its two large faces of the slab are served as the cooling surface to dissipate heat efficiently.

Several research work on the thermal effects of the laser crystal has been related to Nd:YLF [10,11,2,12,13]. In the previous work [14], a general theoretical model was established for the end-pumped slab geometry that considers the divergence of the pump beam, the temperature, and stress distributions, while the focal length of the thermal lens are solved analytically. An accurate numerical solution on Nd:YVO_4 slab is also obtained in Ref. [14], but the thermal effects of the diode-end-pumped Nd:YLF slab have not been discussed sufficiently. In this paper, using the 3D finite element analysis (FEA), we carry out a detailed investigation of the thermal stress effects of the Nd:YLF

* Corresponding author. Tel.: +86 10 62772686; fax: +86 10 62781604.
E-mail address: mazhe@mails.tsinghua.edu.cn (Z. Ma).

0030-4018/$ - see front matter © 2008 Elsevier B.V. All rights reserved.
doi:10.1016/j.optcom.2008.03.012

slab under diode laser end-pumping for both lasing and non-lasing conditions. We focus on the thermal fracture damage of the Nd:YLF slab, which is significantly influenced by the additional heat load generated by upconversion under non-lasing conditions. Likewise, the predicted values are compared with the experimental results.

2. Numerical model

In the previous experimental work [8], Nd:YLF slab was pumped by a pulsed 8-bar laser diode stack with the wavelength of 792 nm. In our recent work, two Nd:YLF slabs inside one resonator was pumped by a CW diode stack with the wavelength of 806 nm, respectively [9]. It has been shown that this new design can improve the conversion efficiency and power scaling and get a higher repetition-rate Q-switched pulse. Therefore, it is very meaningful to establish the numerical thermal model based on the latter pump configuration.

The geometry of the diode-end-pumped Nd:YLF slab is shown in Fig. 1. The slab of dimensions 12 mm × 1 mm × 10 mm is pumped from the end face ($z = 0$) by a 4-bar diode stack. The coupling system is the same as that used in Refs. [5–8]. The optical axis of the crystal is along x direction or y direction. The direction of the output laser beam is the same as the pump beam. The pump beam, propagating through the slab, is shown in Fig. 2. In the slab crystal, the intensity of the pump beam is approximately homogeneous along the x direction. Likewise, as in Ref. [14], the propagation of the shaped pump beam can be approximately described as a high order Gaussian beam using the M^2 factor [15]. The spot size as a function of the distance from the beam waist expands as a hyperbola, which has the form

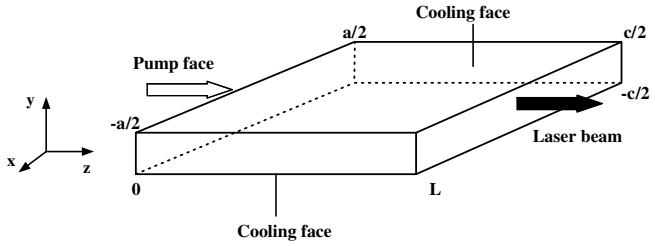

Fig. 1. Schematic diagram of the partially end-pumped slab crystal.

$$\omega(z) = \omega_0 \sqrt{1 + \left[\frac{M^2 \lambda_p (z - z_0)}{n\pi\omega_0^2}\right]^2}, \tag{1}$$

where ω_0 is the waist of the pumping beam, λ_p is the pumping wavelength of free space, and n is the refractive index of the slab. The distance between the beam waist ($\omega_0 \approx 120$ μm) and the pump entrance face is about 2 mm ($z_0 \approx 2$ mm). From Eq. (1) with $M^2 \approx 50$, the width of the pump line at the $z = 0$ face is about 0.4 mm, which is satisfied to matching the cavity mode. In fact, the intensity distribution of the pump beam along the y direction is complicated, but near the waist of the pumping beam, the intensity distribution along the y direction approaches the basic mode Gaussian distribution. Because the waist of the pumping beam is close to the $z = 0$ face, and pump energy is mainly absorbed near the pump entrance face, we then are able to use the basic mode Gaussian distribution to approximately describe the pump intensity distribution along the y direction in the slab.For the heat conductivity coefficients of Nd:YLF along the axis of x, y and z are nearly the same, the general steady-state heat conduction equation for Nd:YLF is

$$\frac{\partial^2 T}{\partial x^2} + \frac{\partial^2 T}{\partial y^2} + \frac{\partial^2 T}{\partial z^2} = -\frac{Q(x,y,z)}{k}, \tag{2}$$

where k is the heat conductivity coefficient of Nd:YLF, $Q(x,y,z)$ denotes the heat generation per unit volume, and T is the temperature. Based on the analyses in the previous paragraph, the total heat load can be written as

$$Q(x,y,z) = C \exp\left[-\frac{2y^2}{\omega^2(z)} - \alpha z\right], \tag{3}$$

where α is the pump absorption coefficient, and constant C can be determined by the following formula

$$C = \frac{\eta P_{ab}}{a \int_{-c/2}^{c/2} \int_0^L \exp\left[-\frac{2y^2}{\omega^2(z)} - \alpha z\right] dy dz} \tag{4}$$

where η is the heat generating efficiency, and P_{ab} is the total absorbed pump power. Under the lasing conditions, the total heat generating efficiency is $\eta \approx 1 - \lambda_p/\lambda_{laser}$. It was shown that the upconversion of Nd:YLF is responsible for significant additional heat load under non-lasing conditions [2]. Therefore, the total heat generating efficiency under non-lasing conditions, when the Q-switch is shut down, is much larger than that under lasing condition.

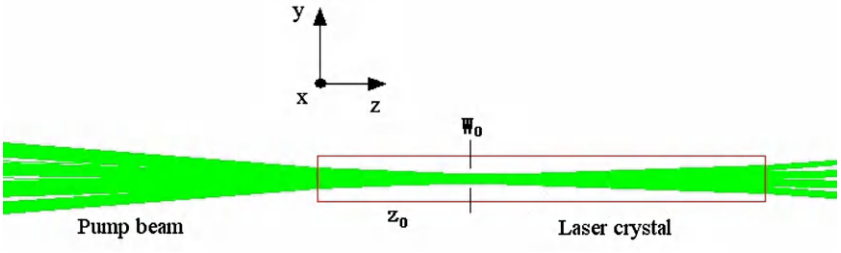

Fig. 2. Simulated pump beam propagating through the slab.

Table 1
Physical properties of Nd:YLF crystal

Young's modulus	$E = 8.5 \times 10^{10}$ Pa
Poisson ratio	$v = 0.33$
Pump wavelength	$\lambda_p = 806$ nm
Laser wavelength	$\lambda_l = 1047$ nm
Doping concentration of Nd^{3+}	1.0%
Refractive indices	$n_a = 1.448$, $n_c = 1.470$ (@1047 nm)
Thermal optical coefficient	$dn_a/dT = -2.0 \times 10^{-6}$/K, $dn_c/dT = -4.3 \times 10^{-6}$/K
Thermal expansion coefficient	$\alpha'_c = 8.3 \times 10^{-6}$/K, $\alpha'_a = 13.3 \times 10^{-6}$/K
Thermal conductivity	$k = 6.0$ W/(m K)
Absorption coefficient	$\alpha = 2.4$ cm^{-1} @806 nm, $E//c$ or $E \perp c$
Cooling temperature	$T_0 = 293$ K

In the absence of the thermal loading, the slab is assumed to be stress-free and not constrained by external forces. The thermal induced stress distributions are generated by the temperature gradients. The stresses, strains, and temperature of the orthotropic crystal are related by the generalized Hooke's laws

$$\varepsilon_{xx} = \frac{\partial u}{\partial x} = \frac{1}{E}[\sigma_{xx} - v(\sigma_{yy} + \sigma_{zz})] + \alpha'_x T, \tag{5a}$$

$$\varepsilon_{yy} = \frac{\partial v}{\partial y} = \frac{1}{E}[\sigma_{yy} - v(\sigma_{zz} + \sigma_{xx})] + \alpha'_y T, \tag{5b}$$

$$\varepsilon_{zz} = \frac{\partial \omega}{\partial x} = \frac{1}{E}[\sigma_{zz} - v(\sigma_{xx} + \sigma_{yy})] + \alpha'_z T, \tag{5c}$$

$$\gamma_{xy} = \frac{\tau_{xy}}{G}, \gamma_{yz} = \frac{\tau_{yz}}{G}, \gamma_{zx} = \frac{\tau_{zx}}{G} \tag{5 d}$$

where E is Young's modulus, G is modulus of elasticity in shear, v is Poisson's ratio, α'_x, α'_y and α'_z are the thermal expansion coefficient, σ_{xx}, σ_{yy} and σ_{zz} are the direct stresses, ε_{xx}, ε_{yy} and ε_{zz} are direct strains, τ_{xy}, τ_{yz} and τ_{zx} are the shear stresses, γ_{xy}, γ_{yz} and γ_{zx} are the shear strains.

The values for all the parameters of Nd:YLF used for calculation are summarized in Table 1. In our experiment [9], the Nd:YLF slab is with 1% doping concentration. Under the pump beam polarization direction of $E//a$ or $E//c$, the absorption coefficients of the slab at 806 nm are nearly the same, about 2.4 cm^{-1}. Considering the two larger cooled faces have a good thermal contact with a water-cooled heat sink, we assume that the cooled faces are to be maintained at constant cooling temperature T_0 and neglect the heat flows from the non-cooled faces. Using the boundary conditions, the temperature and thermal stress distributions can be numerically achieved by solving Eqs. (2), (3) and (5).

3. Numerical results

The approximate solution of the temperature and thermal stress can be achieved using the analytical method as shown in Ref. [14]. In this paper, we carry out the numerical solution which is much accurate than the analytical solution. First, we consider the same situation as that which is used in Ref. [9]. The optical axis of the Nd:YLF slab is along the y direction (Case 1), and the output laser beam is of vertical polarization. The thermal and mechanical boundary conditions are the same as Section 2, and the water-cooling temperature is $T_0 = 293$ K. Under lasing conditions, the heat generating efficiency is about 23% ($\eta \approx 23$). Ref. [2] showed that the heat dissipation efficiency of Nd:YLF under non-lasing conditions increases nonlinearly with pump power and can exceed 50%. At the maximum absorbed pump power of 140 W, we shall assume the heat generating efficiency of $\eta \approx 50$ under the non-lasing conditions in our calculation. Because of the symmetrical characteristic of the slab, we take the symmetrical quarter of the slab (6 mm × 0.5 mm × 10 mm) to do meshing and numerical calculation. The 3D finite element analysis (FEA) is used to solve the problem.

Figs. 3 and 4 show the 3D numerical temperature distributions for both lasing and non-lasing conditions. The maximum temperature rise is about 20.7 K at the pump entrance face under the lasing conditions, while that is 45 K under the non-lasing conditions. Therefore, the thermal stresses induced by the temperature rise in the end-pumped Nd:YLF slab are much stronger under the non-lasing conditions. As is shown in Fig. 4, the focusing and divergence process of the pump beam causes the temperature distribution along z axis differs from exponential. The thermal induced stress distributions both along y direction and the z direction are shown in Figs. 5 and 6. The value of σ_{yy} is nearly zero throughout the slab. The shear stresses in the slab are much smaller than all the direct stresses. In Fig. 5, it can be seen that the stress σ_{xx} and σ_{zz} change from compressive in the center to tensile near the cooling surfaces. We focus on the tensile stress on the cooling surface which is more harmful to the fraction of the laser crystal. The maximum σ_{xx} is about 32.5 MPa near the position of $z = 0.8$ mm, and there the maximum σ_{zz} is about 34 MPa (The fracture stress of Nd:YLF is about 33 MPa [16]). The values of the tensile

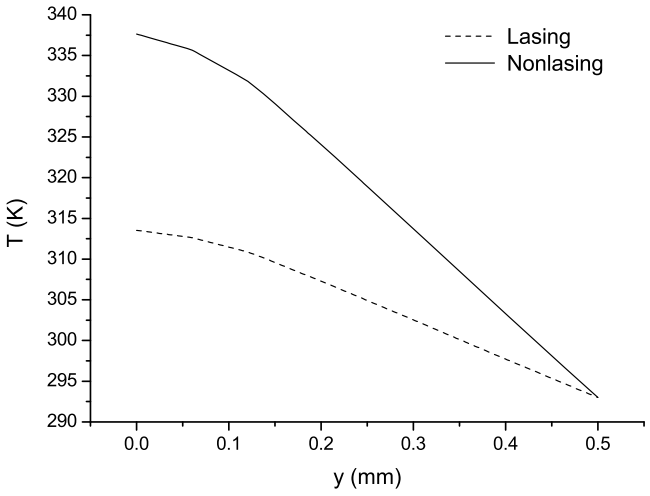

Fig. 3. Temperature distributions along y axis at $z = 0$.

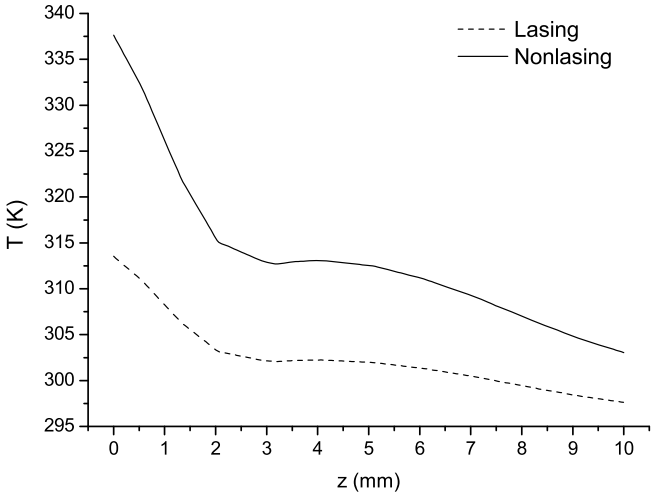

Fig. 4. Central temperature along z axis.

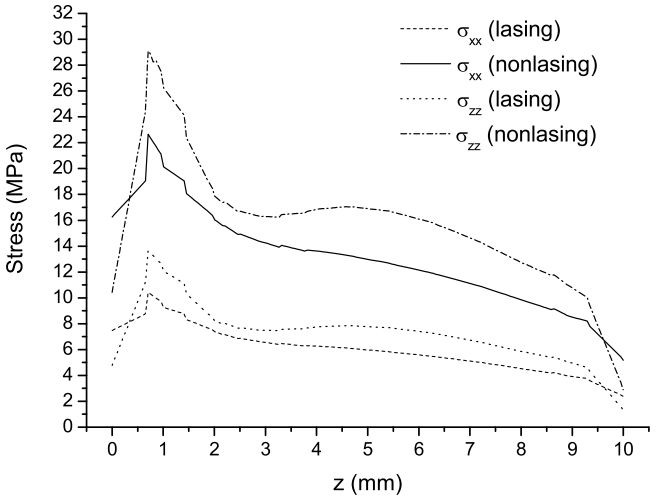

Fig. 7. Stress distributions along z axis on the cooling surface of the slab (Case 2).

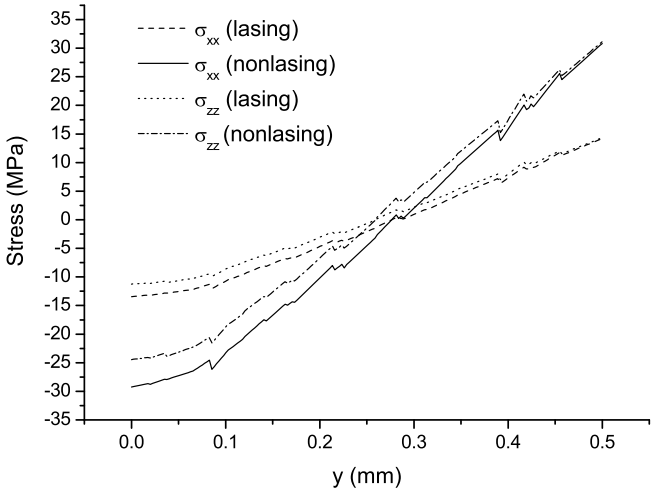

Fig. 5. Stress distributions along y axis at $z = 0.8$ mm (Case 1).

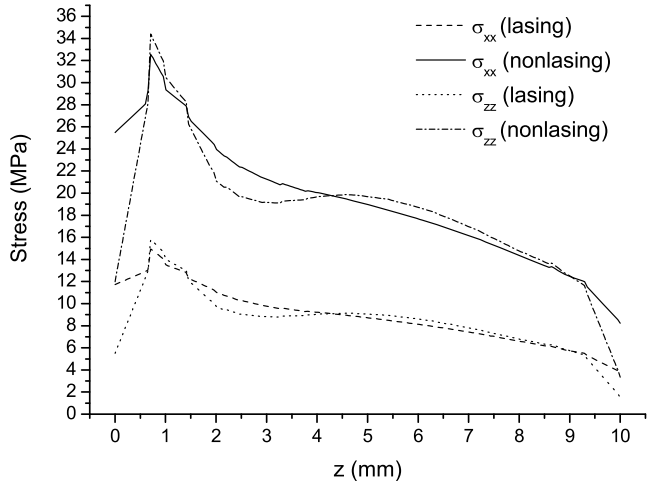

Fig. 6. Stress distributions along z axis on the cooling surface of the slab (Case 1).

stresses under non-lasing conditions are much larger than those under the lasing conditions. It predicts that the fraction in the slab may more easily take place under the non-lasing conditions.

The thermal expansion coefficient of the Nd:YLF along the optical axis is smaller than that vertical to the optical axis. Therefore, if the optical axis of Nd:YLF is along y direction (Case 2), the maximum stress can be reduced a lot under the same pump power. In this case, the output laser beam is of horizontal polarization. The temperature distribution in the two cases is nearly the same. Fig. 7 shows the calculated stress distribution in Case 2 under the pump power 140 W. Under non-lasing conditions, the maximum stress σ_{zz} and σ_{xx} reduce to about 28 MPa and 22 MPa, respectively.

For the Nd:YLF crystal, the maximum surface stress at which fracture occurs is about 33 MPa. As a result, in Case 1, when we increase the total pump power to about 140 W, the fracture may occur on the Nd:YLF slab. In comparison, the fracture may occur under a higher pump power more than 150 W applied on the slab in Case 2. The experiment results will be shown in next section. The non-continuous appearance of the stresses is a computational artifact caused by the meshing algorithm in the finite element analysis. If the meshes are denser, these non-continuous will be less.

4. Experiment results

The thermal lensing of the Nd:YLF slab is small, and we focus on the thermal fracture damage of the slab. When the laser output is operated on CW mode (lasing conditions), the fracture of the crystal never occurs at the pump power of 140 W. When we close the Q-switch (non-lasing conditions) and increase the pump power to about 135 W, thermal fracture damage of the Nd:YLF slab (case 1) takes place. Fig. 8 shows the typical mechanical destroyed

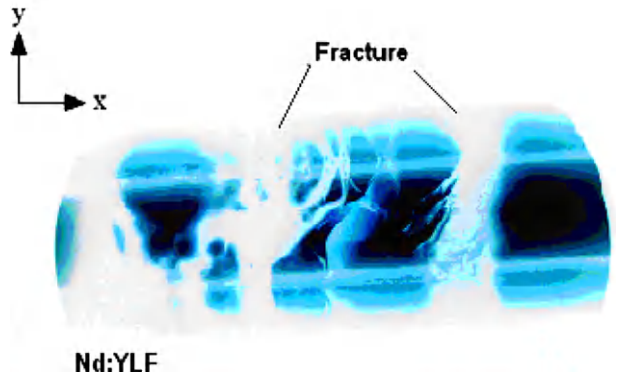

Fig. 8. Photograph of the thermal fracture damaged Nd:YLF slab.

Nd:YLF slab. The position of the fracture is on the cooling surface and about 0.9 mm away from the pump entrance face. The facture direction is complex and it is quite different from that of the Nd:YVO_4 slab [14]. It indicates that the damage is caused by both σ_{xx} and σ_{zz}. For comparison, facture never occurred in Nd:YLF slab in Case 2 under the same pump power. The experiment results are agreed with the numerical solution.

5. Conclusions

In the present work, an accurate numerical model and its 3D FEM solutions for the thermal stress analysis of the high-power end-pumped Nd:YLF slab has been investigated. Our analyses contain both the lasing and non-lasing conditions for comparison. Under the non-lasing conditions, the much larger thermal stresses is much harmful to Nd:YLF slab. From these results, we also find that the Nd:YLF slab can be operated under different maximum pump power with different optical axis orientation. Experimental investigations have also been presented for comparison and are agreed well with numerical results. These results discussed in this paper will be helpful to guide the design of diode-end-pumped solid-state lasers.

References

[1] W. Koechner, Solid-state Laser Engineering, fifth ed., Springer-Verlag, Berlin, 1999.
[2] M. Pollnau, P. Hardman, M. Kern, W. Clarkson, D. Hanna, Phys. Rev. B 58 (1998) 16076.
[3] K. Du, N. Wu, J. Xu, J. Giesekus, P. Loosen, R. Poprawe, Opt. Lett. 23 (1998) 370.
[4] K. Du, D. Li, H. Zhang, P. Shi, X. Wei, R. Diart, Opt. Lett. 28 (2003) 87.
[5] H. Zhang, P. Shi, D. Li, K. Du, Appl. Opt. 42 (2004) 1681.
[6] P. Shi, D. Li, H. Zhang, Y. Wang, K. Du, Opt. Commun. 229 (2004) 349.
[7] H. Zhang, K. Du, D. Li, et al., Appl. Opt. 43 (2004) 2940.
[8] H. Zhang, D. Li, P. Shi, R. Diract, A. Shell, C.R. Haas, K. Du, Opt. Commun. 250 (2005) 157.
[9] D. Li, Z. Ma, R. Haas, A. Shell, J. Simon, R. Diart, P. Shi, P. n Hu, P. Loosen, K. Du, Opt. Lett. 32 (2007) 1272.
[10] J. Murray, IEEE J. Quantum Electron. 19 (1983) 488.
[11] C. Pfistner, R. Weber, H. Weber, S. Merazzi, R. Gruber, IEEE J. Quantum Electron. 30 (1994) 1605.
[12] A. Andrade, T. Catunda, I. Bodnar, J. Mura, M. Baesso, Rev. Sci. Instrum. 74 (2003) 877.
[13] R.L. Aggarwal, D.J. Ripin, J.R. Ochoa, T.Y. Fan, J. Appl. Phys. 98 (2005) 103514.
[14] Z. Ma, D. Li, J. Gao, N. Wu, K. Du, Opt. Commun. 275 (2007) 179.
[15] T. Taira, J. Saikawa, T. Kobayashi, R.L. Byer, IEEE J. Sel. Top. Quantum Electron. 3 (1997) 100.
[16] <http://www.st.northropgrumman.com/synoptics/products/laser/NdYLF.html>.